Dielectric study of a subphase stabilized in an exceptionally wide temperature range by a delicate balance of interlayer interactions and thermal fluctuations

Zhengyu Feng,[1] Vigneshwaran Swaminathan,[2,*] Vitaly P. Panov,[2,3] Atsuo Fukuda,[2] Ken Ishikawa,[1,†] and Jagdish K. Vij[2,‡]

[1]*Department of Materials Science and Engineering, School of Materials and Chemical Technology, Tokyo Institute of Technology, 2-12-1 S8-Ookayama, Meguro-ku, Tokyou 152-8552, Japan*

[2]*Department of Electronic and Electrical Engineering, Trinity College Dublin, The University of Dublin, Dublin 2, Ireland*

[3]*Department of Electronic and Computer Engineering, Sungkyunkwan University, Suwon 440-476, South Korea*

(Received 3 April 2020; accepted 30 June 2020; published 22 July 2020)

The chiral smectic phases of calamitic liquid crystals, SmC^* and SmC_A^*, are characterized by the synclinic *ferroelectric F* ordering and the anticlinic *antiferroelectric A* ordering in adjacent layers. Various states with mixed *A* and *F* orderings are degenerate at the frustrated phase-transition point. The degeneracy lifting is commonly caused by the long-range interlayer interactions (LRILIs), producing a series of biaxial subphases specified by a relative ratio of both orderings, $q_T = [F]/([A] + [F])$. Sandhya *et al.* [Phys. Rev. E **87**, 012502 (2013)] established, however, the importance of thermal fluctuations in the degeneracy lifting in some binary mixtures of MC881 and MC452. They observed the most intriguing interplay of thermal fluctuations and LRILIs in the stabilization of an apparently single subphase. Since no other detailed experimental study of the subphase has so far been made, we carry out its dielectric investigations and clarify the following five points: (1) the subphase is surely a single phase from $\approx 80\,^{\circ}$C down to room temperature; (2) the imaginary part of complex permittivity ϵ'' shows the weak antiphase mode and hence it must be antiferroelectric $q_T = 1/2$; (3) ϵ'' becomes much stronger above $\approx 80\,^{\circ}$C, indicating the emergence of ferroelectric and/or ferrielectric states; (4) the dielectric amplitude gradually increases at least just above the 1/2 subphase, suggesting it be due to a continuous increase of q_T; and (5) at low temperatures the antiphase relaxation mode shows irregularities that indicate the important role played by the cooperative motion of the layer undulation as well as of the director tilting.

DOI: 10.1103/PhysRevE.102.012703

I. INTRODUCTION

The ferroelectricity and antiferroelectricity have been found in the smectic phases of SmC^* and SmC_A^*, respectively, in chiral calamitic liquid crystals [1,2]. The tilting ordering between adjacent layers is anticlinic antiferroelectric in SmC_A^*, whereas it is synclinic ferroelectric in SmC^*. Hereafter we use abbreviations, *A* ordering and *F* ordering, respectively. At the phase transition temperature T^*, i.e., the frustration point, various states with mixed *A* and *F* orderings are degenerate. Long-range interlayer interactions (LRILIs) or thermal fluctuations may lift the degeneracy [3,4]; the resulting states are specified by the relative ratio of *A* and *F* orderings [5], $q_T = [F]/([A] + [F])$. The nature of many subphases was initially explained by using the axial next-nearest-neighbor Ising model in magnetism [6–8]. In this treatment, thermal agitations required the spins to flip between the ± 1 states (representing SmC_A^* and SmC^*, respectively) so that a variety of subphases are certain to emerge. In liquid crystals, however, thermal transition between SmC_A^* and SmC^* can hardly occur, when they are separated by a finite potential barrier. Even when the temperature-induced phase transition is observed directly between SmC_A^* and SmC^*, it is caused nonuniformly by the solitary wave propagation [9] but not uniformly by the thermal excitation of cooperative director motion of antiphase mode [10–14]. Usually we resort to the absolute zero temperature approximation in liquid crystals. In fact, a variety of optically biaxial polar subphases between the main phases, SmC_A^* and SmC^*, observed experimentally have been ascribed to the degeneracy lifting at the frustration point due to LRILIs [3–5]. It was considered not easy at the time to find out LRILIs in polar smectics, where no truly positional order exists. Nevertheless Osipov and Fukuda [15] introduced a fundamental concept of discrete flexoelectric effect in 2001 for the first time. Based on this seminal effect, Emelyanenko and Osipov [16] devised intriguing and useful effective LRILIs. Their theoretical framework with a reasonably large, virtually constant tilt angle can roughly explain not only the experimentally observed subphase emerging sequence in a temperature range far away from the SmC^*-Sm*A* transition point [17], SmC_A^*-1/4-1/3-2/5-3/7-1/2-SmC^*, but also their nonplanar superlattice structures with highly distorted nanometer-sized helicoidal director arrangements in the unit cells [18–24]. In this way, it has been generally considered that the successive

*Present address: Division of Physics, Vellore Institute of Technology, Chennai Campus 600127, India.

†Corresponding author: ishikawa.k.ab@m.titech.ac.jp

‡Corresponding author: jvij@tcd.ie

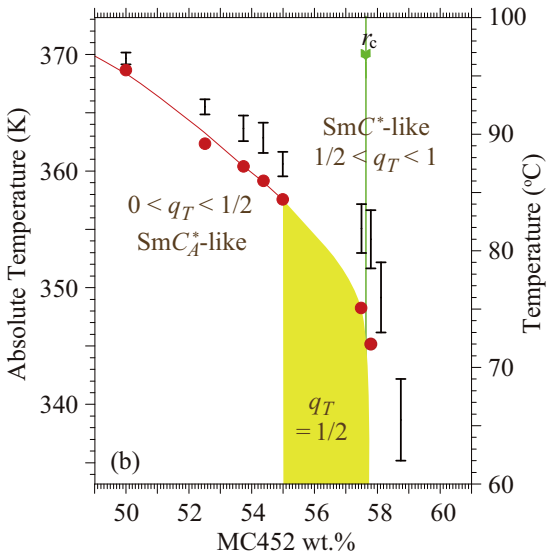

FIG. 1. Peculiar bulk phase diagram of MC881-MC452 binary mixture system near the critical concentration $r_c = 57.65 \pm 0.15$ wt %, reproduced from Figs. 4 and 5 of Ref. [25]. The bulk phase diagram was obtained by observing Bragg reflection spectra due to the director helical structure. Bars indicate the temperature ranges where the full-pitch band gradually grows and circles specify the half-pitch divergence temperatures. An apparently single subphase emerges in a narrow concentration $r \leqslant r_c$ range of less than 3 wt %.

transitions via the main phases and subphases are of first order and are characterized by abrupt changes because of the degeneracy lifting due to the effective LRILIs at the frustration point.

Unexpectedly, however, Sandhya *et al.* [25–27] found that the change from SmC_A^* to SmC^* induced by temperature is continuous in the bulk of some binary mixtures of MC881 and MC452. Up to that time Song *et al.* had studied the dielectric response together with electric-field-induced birefringence (EFIB) and obtained the ordinary bulk phase diagram of the MC881-MC452 mixture system, without noticing any irregular continuous change, as shown in Fig. 3 of Ref. [28]. The phase emerging sequence is SmC_A^*-SmA-Iso in pure MC881, whereas it is SmC^*-Iso in pure MC452. As the MC452 concentration increases, apparently SmC^* comes to emerge above SmC_A^*, but the borderline between SmC_A^* and SmC^* appears to become parallel to the temperature axis at the critical concentration r_c. It should be noted that the three-layer ferrielectric $q_T = 1/3$ subphase was initially suggested to exist in a narrow concentration range of $r \lesssim r_c$; moreover, SmC_A^* does not seem to exist as a low-temperature phase of SmC^* for $r \gtrsim r_c$. The free energy difference between SmC_A^* and SmC^* must be extremely small in a wide temperature range near the vertical borderline at r_c. Following these findings, Sandhya *et al.* [25–27] carefully studied the mixture in the concentration range around r_c by using Bragg reflection spectra caused by the director helical structure and obtained the bulk phase diagram as reproduced in Fig. 1. They confirmed the observation of a continuous change from SmC_A^* to SmC^* together with the emergence of a single subphase at around 56 wt %. The Bragg reflection is observed favorably in the near-UV, visible, or near-IR wavelength region in the almost entire temperature range covering the apparently SmC_A^* and SmC^* phases and in-between. The half-pitch band of SmC_A^* in pure MC881 is observed at about 0.4 μm and that of the subphase with exceptionally wide temperature stability range near the critical concentration r_c appears at about 1 μm. On the low concentration side of the subphase, the Bragg reflection peak wavelength characteristically becomes longer continuously with temperature, diverges with a change of its handedness, and decreases to attain the visible wavelength of the apparently SmC^* half-pitch reflection band. The full-pitch band emerges accordingly in the apparently SmC^* temperature range, but peculiarly its emergence does not change the handedness of the half-pitch band [29–31]. Even more peculiarly, it does not appear abruptly but emerges gradually; the growing temperature range becomes wider near the critical concentration r_c of the mixture.

Sandhya *et al.* tried to explain the continuous peak wavelength change of the half-pitch band and the gradual growth of the full-pitch band, noticing that the absolute zero temperature approximation would not hold anymore. They assumed a thermal equilibrium between the synclinic and anticlinic orderings and the resulting Boltzmann distribution for the ratio between the orderings $[A]/[F] = \exp\{-\Delta E/(k_B T)\}$ where ΔE is usually considered to change linearly with temperature near the frustration point; the thermal equilibrium is considered to be attained in a nonuniform defect-assisted way through solitary waves moving around dynamically [9]. The experimentally observed Bragg reflection peak versus temperature is rather well reproduced at least on the high-temperature side of the pitch divergence for $r < r_c$. Furthermore, the analysis based on the degeneracy lifting due to thermal fluctuations can explain that the full-pitch band begins to grow characteristically at about $q_T \approx 0.991$ on both high and low concentration sides of the single subphase around 56 wt %; in other words, only 1% thermally excited anticlinic defects suppress the emergence of the full-pitch band in apparently SmC^*.

On the low-temperature side of the divergence, on the other hand, the experimentally observed peak wavelength versus temperature curve could hardly be reproduced, except for the long-wavelength part corresponding to the narrow temperature range of $q_T > 1/2$. Furthermore, the single subphase emerges in an exceptionally wide temperature range from 80 °C down to the room temperature or lower for a concentration $r \leqslant r_c$ range as narrow as less than 3 wt %. It is natural to consider that the interplay between thermal fluctuations and LRILIs produces those observed characteristic phenomena. Now a critical issue is raised: What is the subphase with the exceptionally wide temperature range of stability? Sandhya *et al.* suggested that it should be either $q_T = 1/3$ or $1/2$, but did not assertively conclude which of the two is correct, although they inclined toward $1/2$ on the basis of the characteristic g-$\tilde{T}$ phase diagram obtained by Emelyanenko and Osipov [16,32]. In the 25th International Liquid Crystal Conference (Dublin, 2014) one of the authors pushed forward the inclination to $1/2$, insisting the notion of thresholdless antiferroelectricity reported in 1995 in connection with the application to gray-scale liquid-crystal displays [27,33]. Actually MC881 and MC452 were developed by MGC (Mitsubishi Gas Chemical Co., Inc.) and the binary mixtures at around r_c were reported to show the thresholdless, hysteresis-

free, V-shaped switching in thin cells [34,35]. It is legitimate to consider that the subphase with the exceptionally wide temperature range of stability found by Sandhya *et al.* must play an important role in the intriguing switching property of the thin cells.

Since little is known about the subphase, we studied its dielectric properties as a first step in this paper. The following five points are clarified: (1) the subphase is surely a single phase from $\approx 80\,^{\circ}$C down to room temperature; (2) the imaginary part of complex permittivity vs frequency $\epsilon''(f)$ apparently shows the weak antiphase mode and hence it must be the antiferroelectric $q_T = 1/2$ with the four-layer unit cell (hereafter simply designated as the $q_T = 1/2$ subphase); (3) $\epsilon''(f)$ becomes much stronger above $\approx 80\,^{\circ}$C, indicating the emergence of ferroelectric and/or ferrielectric states (the SmC^*-like phase); (4) the peak intensity gradually increases at least just above the $q_T = 1/2$ subphase, suggesting a continuous increase in q_T with temperature; and (5) at temperatures below $0\,^{\circ}$C and at low frequencies, the antiphase relaxation mode shows some irregularities, which indicate the important role played by the cooperative motion of the layer undulation as well as of the director tilting.

II. EXPERIMENTS

The samples used are two binary mixtures of antiferroelectric MC881 containing ferroelectric MC452, the concentrations of which are 55.09 and 55.70 wt %, respectively. Their chemical structures are given in Fig. 2. For making dielectric spectroscopic measurements of the confined LC samples, planar and homeotropic aligned liquid-crystalline cells are constructed so that smectic layers are almost perpendicular and parallel to the cell surface, respectively. Indium tin oxide (ITO) –coated glass plates form the electrodes of the cells. The ITO-coated glass plates having relatively low sheet resistance of ($10\Omega/\square$) are used, which sometimes produces a spurious resonance peak observed at near 3 MHz. The cell spacing was fixed at 28 ± 2 μm in each case by using thin Mylar film spacers; the cell size is about 10 mm $\times$ 10 mm and its capacitance is about 30 pF. The planar alignment was achieved by spin-coating the ITO electrodes with RN1175 (Nissan Chemical Corporation, Japan) polymer solution. The polymer layer was cured at a temperature of $250\,^{\circ}$C for 1 h in a vacuum oven, where the wet layer of the solution is imidized. The thickness of an alignment layer of a planar cell is about 10 nm and after its curing the alignment layer is rubbed unidirectionally for achieving the directional alignment of the molecular director. The homeotropic alignment has similarly been achieved by spin coating CYTOP^{TM} (AGC Chemicals)

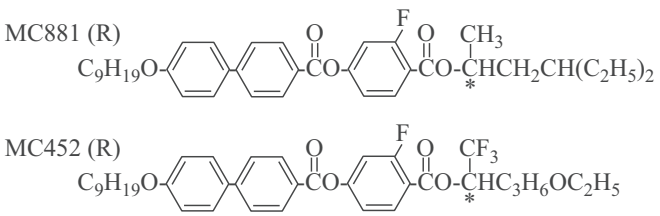

FIG. 2. The chemical formula for MC881 and MC452, both of which are (*R*) moieties.

TABLE I. Summary of four measurements (1)–(4) actually performed. The MC452 concentrations are 55.09 wt % in measurement (1) and 55.70 wt % in the others, (2)–(4).

No.	Alignment	Thickness (μm)	Temp. ($^{\circ}$C) Range	Step	Freq. (Hz) Range
(1)	Planar	29	30 to 110	0.5	40–10M
(2)	Planar	26	−30 to 20	5	1–10M
			20 to 115	1	
(3)	Planar	29	−30 to 115	2	0.1–10M
(4)	Homeo.	30	−30 to 118	2	0.01–10M

on the ITO-coated glass substrates. Dielectric measurements were carried out by slowly heating sample cells using an HP4192A impedance analyzer (40 Hz–10 MHz frequency range) or a Novocontrol Broadband alpha high-resolution dielectric analyzer (0.01 Hz–10 MHz frequency range). The real and imaginary parts of the complex permittivity were obtained both for the planar and the homeotropic cells as summarized in Table I under slow heating at a rate of $0.2\,^{\circ}$C/min.

Since the probe field is weak enough (0.05 V/μm), both the real and the imaginary parts of the complex permittivity correspond to a linear change in the induced polarization brought about by the applied field. In order to determine the dielectric amplitude $\Delta\epsilon_j$ and the relaxation time τ_j of each relaxation mode, the dielectric spectra are analyzed using the Havriliak-Negami equation that expresses complex permittivity $\epsilon(\omega)$ in terms of the various relaxation processes,

$$\epsilon(\omega) = -\frac{i\sigma_0}{\epsilon_0\omega} + \epsilon_\infty + \sum_{j=1}^{n} \frac{\Delta\epsilon_j}{\{1 + (i\omega\tau_j)^{\alpha_j}\}^{\beta_j}}. \qquad (1)$$

Here $\Delta\epsilon_j$, τ_j, α_j, β_j, and ϵ_∞ correspond to dielectric amplitude, relaxation time, Havriliak-Negami distribution parameters, and infinite frequency relative permittivity, respectively; $\sigma_0/\epsilon_0\omega$ is the contribution of ions to the dielectric loss of the medium where ϵ_0 is the permittivity of the free space; and n is the number of relaxation processes up to 4. These parameters are found by the fitting of the experimental data of $\epsilon(\omega)$ to Eq. (1) using the WinFIT program purchased from Novocontrol GmbH, Germany. We also find $\Delta\epsilon_j$ and τ_j as a function of temperature. Frequency of the jth relaxation process is related to τ_j by $f_j = 1/(2\pi\tau_j)$. If α_j, β_j are both equal to unity for a process under discussion, then that particular process is named Debye, otherwise the process is known as Havriliak-Negami or Cole-Cole. For the case of the Debye process, $\Delta\epsilon_j = 2\epsilon''_{j,\max}$. The ions in the liquid crystal give rise to dielectric loss in addition to the dipolar loss; the dielectric loss due to ions decreases with an increase in frequency of the alternating field on the $\log_{10}$-$\log_{10}$ scale. The ions continually lag behind alterations of the probe field as its frequency progressively increases. Furthermore, in order to make electrical contacts of the probe generator to the two electrodes of the cell, there is a need to use conducting ITO electrodes. The gold or silver electrodes are ideal to use in a dielectric experiment but these are avoided here since these electrodes are not transparent to light in the visible range for optical polarizing microscopy. The conducting layer acting in series with the cell capacitance gives rise to a dielectric

loss peak. The reciprocal of the product of resistance per square of the ITO coating with the cell capacitance equals the angular frequency of the ITO loss peak. This peak is easily distinguishable as its frequency does not change much with temperature.

III. RESULTS

Let us begin with the frequency dependence of the imaginary part of complex permittivity $\epsilon''(f)$ in planar cells. Figure 3 summarizes $\epsilon''(f)$ at various representative temperatures in measurements (1) and (2) listed in Table I. Figure 3(a) illustrates $\epsilon''(f)$ in the highest temperature range investigated. The sample is in Sm*A* at 110 °C and it becomes the isotropic phase at about 113 °C. A relaxation peak around 1 MHz is observed in Sm*A* just below the isotropic phase; the peak frequency gradually decreases down to 0.1 MHz with the peak intensity increasing by more than three times at 107 °C, where two peaks are clearly observed indicating some phase coexistence. In the SmC^*-like phase below about 107 °C, the peak intensity is more than 100 with the peak frequency of about 3 kHz. For lower temperatures as shown in Fig. 3(b), both the intensity and frequency of the loss curves do not change much until about 88 °C, and then the intensity of dielectric loss gradually decreases to a very small value at the transition temperature of about 83.5 °C to the supposedly single subphase with an exceptionally wide stability temperature range. In this subphase temperature range shown in Figs. 3(c) and 3(d), we can see two peaks and tentatively designate them as the medium- and low-frequency relaxation modes observed in the planar cells (hereafter abbreviated as M_p and L_p modes, respectively). Increasing $\epsilon''(f)$ toward lower frequencies is caused by the dc conductivity due to impurity ions contained in the sample, and the L_p mode emerges as a shoulder of this conductivity tail. The M_p mode intensity is larger than that of the L_p mode and both mode frequencies become lower with falling temperature. When the temperature is further lowered, we can see an additional peak on the high-frequency side of the M_p mode as shown in Figs. 3(e) and 3(f). It is tentatively designated as the high-frequency relaxation mode in planar cells (hereafter abbreviated as H_p mode). It becomes conspicuously asymmetric, i.e., the relaxation peak shape deviates from the Debye type as seen in Fig. 3(f). Furthermore the M_p mode intensity keeps increasing with falling temperature and attains more than 10 at −5 °C; at the same time a shoulder appears on the high-frequency side of the M_p mode peak.

Now we move on to the results of a homeotropic cell. Figure 4 summarizes $\epsilon''(f)$ at various representative temperatures in measurement (4) of Table I. At a glance of Figs. 4(a)–4(e), a group of peaks are conspicuous throughout the temperature range investigated. We tentatively designate them as the low-frequency relaxation mode observed in the homeotropic cell (hereafter abbreviated as the L_h mode). In the highest temperature range investigated shown in Fig. 4(a), increasing $\epsilon''(f)$ toward lower frequencies must be caused by the dc conductivity due to impurity ions contained in the sample, which shows a peak with intensity as large as 100 at a very low frequency [36]. The transition from Sm*A* to the isotropic phase occurs between 114 °C and 112 °C; the L_h mode appears around 0.7 MHz with peak intensity of a little

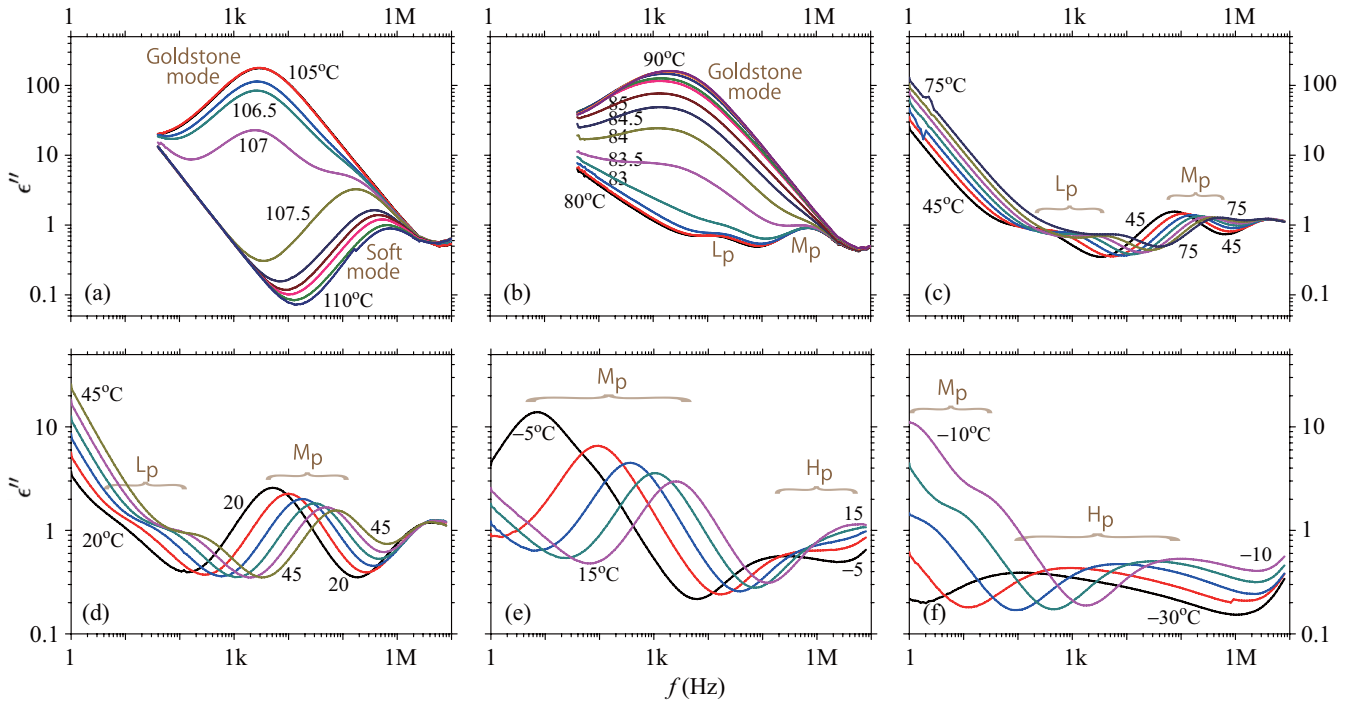

FIG. 3. Temperature variation of the imaginary part of complex permittivity $\epsilon''(f)$ in the planar cell. Temperature ranges and steps are (a) 110 to 105 °C at a step of 0.5 °C, (b) 90 to 80 °C at a step of 1°C with two additional 84.5 and 83.5, and (c)–(f) 75 to − 30 °C at a step of 5 °C. The temperature range of 105 to 90 °C is not plotted here as the peak intensity and the frequency of the dielectric loss curves do not change much in this temperature range. The steps are so chosen that the lines are not too thick but still show a delicate change clearly. See text for further details.

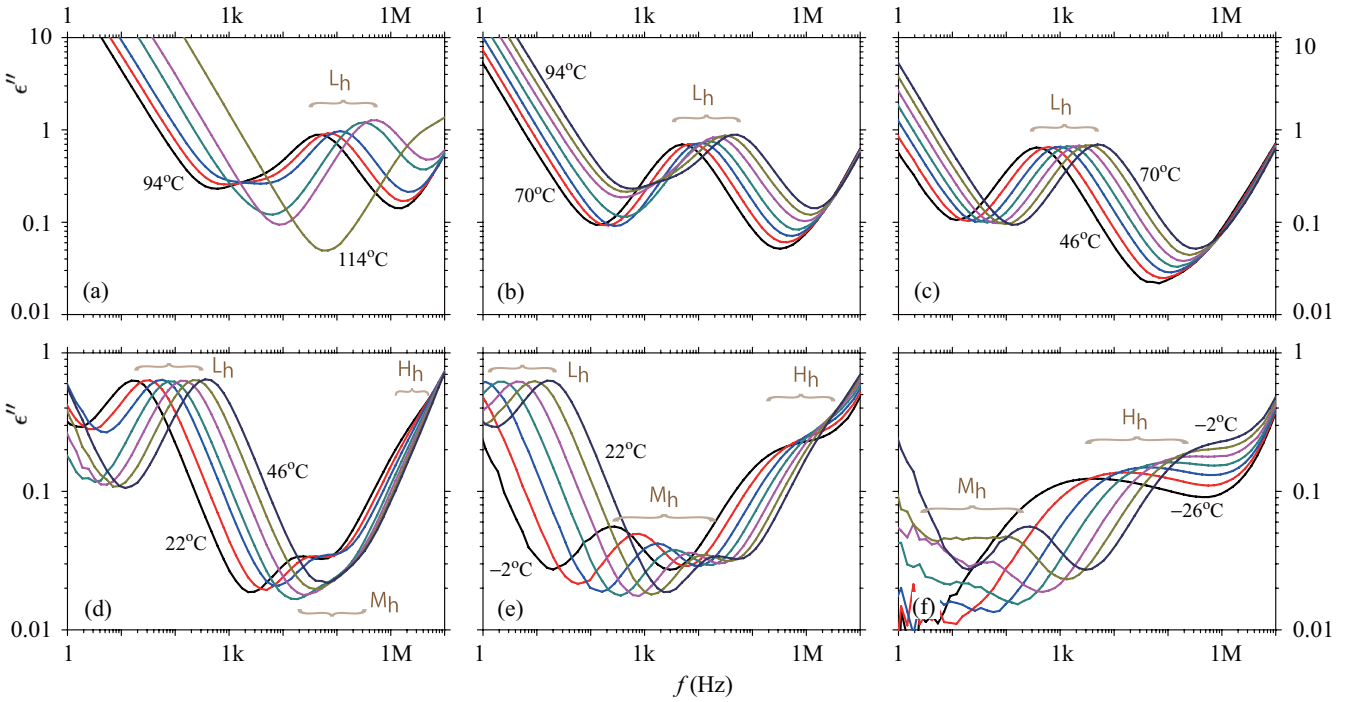

FIG. 4. Temperature variation of the imaginary part of complex permittivity $\epsilon''(f)$ in the homeotropic cell. For plots, a temperature step of 4 °C throughout is chosen such that the lines are not too thick but still a delicate change is shown clearly: (a) 114 to 94 °C, (b) 94 to 70 °C, (c) 70 to 46 °C, (d) 46 to 22 °C, (e) 22 to − 2°C, and (f) −2 to −26°C. See text for further details.

larger than 1 in SmA, and its frequency and intensity slightly decrease with falling temperature. The transition between the SmC^*-like phase and SmA occurs between 102 °C and 106 °C, but neither the peak intensity nor the frequency of the L_h mode shows any big change, although a very small irregularity is discernible. In Fig. 4(b), where the transition occurs from the supposedly single subphase with an exceptionally wide stability (temperature) range to the SmC^*-like phase between 82 °C and 86 °C, we can see the similar irregularity in the frequency and intensity changes of the L_h mode. At lower temperatures as seen in Figs. 4(c) and 4(d), another relaxation mode comes to appear on the high-frequency side of the L_h mode; first it looks like a shoulder of the high-frequency tail and then shows a clear peak. We tentatively designate it as the medium frequency relaxation mode observed in the homeotropic cell (hereafter abbreviated as the M_h mode). It should be noted that a rather conspicuous change is observed between 30 °C and 34 °C as seen in Fig. 4(d). In the much lower temperature range shown in Figs. 4(e) and 4(f) we can see the homeotropic high-frequency relaxation (H_h) mode, the shape of which becomes broad and asymmetric deviating from the Debye type at very low temperatures, likewise in Figs. 3(e) and 3(f).

IV. MODE ASSIGNMENTS

The relaxation frequencies of these modes, L_p, M_p, and H_p in the planar cell and L_h, M_h, and H_h in the homeotropic cell, are plotted as a function of temperature in Fig. 5. The subscripts p and h stand for planar and homeotropic, respectively. Each curve of the three modes in the planar cell almost coincides with the corresponding curve in the homeotropic cell. This means that the three relaxation processes are detected in both the planar and homeotropic cells; hereafter we simply call them L, M, and H, respectively, without adding a subscript p or h. It is well known that there exist two kinds of relaxation processes, noncollective and collective, in SmC^*_A, SmC^*, and subphases between them [10–13]. The liquid-crystal molecule itself can undergo two

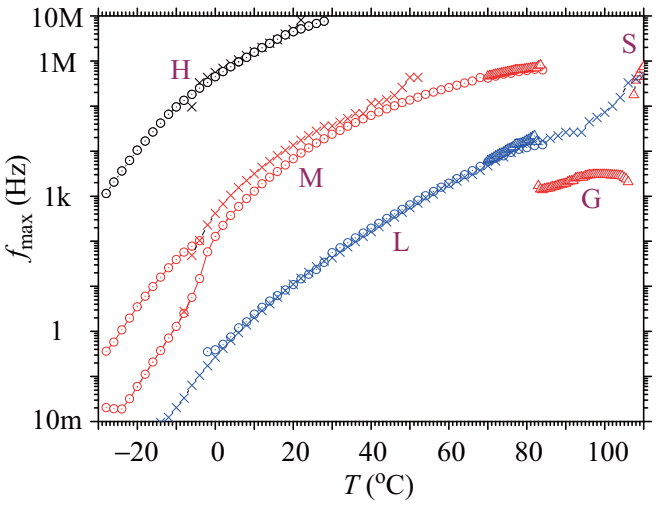

FIG. 5. The relaxation frequency vs temperature $f_{max}(T)$ calculated from the measurements (1) triangle, (3) circle, and (4) cross referred to those in Table I. The high (H), medium (M), and low (L) frequency modes are observed in the $q_T = 1/2$ subphase. G and S refer to the Goldstone and soft modes, respectively. See text for details.

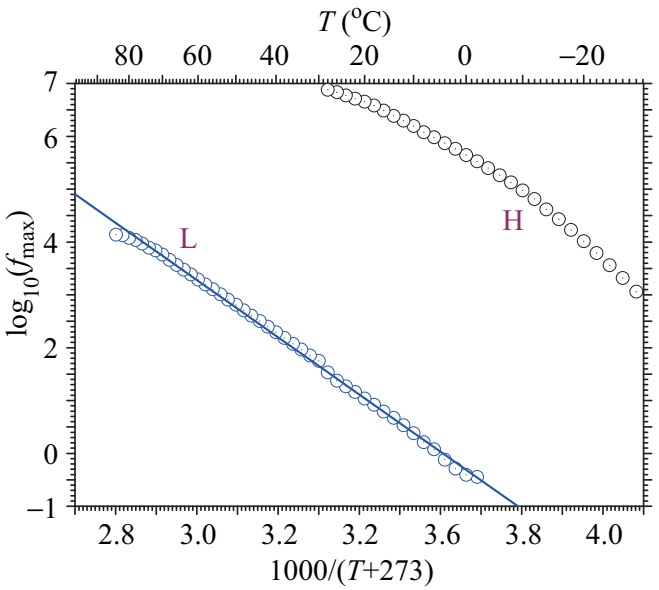

FIG. 6. The Arrhenius behavior of the H and L relaxation processes observed in measurement (3) of Table I and summarized in Fig. 5.

dielectric relaxation mechanisms with different frequencies; one is the high-frequency relaxation mechanism that is connected to the rotation around the long axis and the other is the low-frequency relaxation related to the rotation around its short axes. These relaxations must be noncollective, because the rotational motion of a given single molecule is almost uncorrelated to the motion of all other molecules. By reference to previous investigations, it is legitimate to assign the relaxation processes H and L to the molecular dipole's reorientation processes around the molecular long and short axes, respectively. In fact, the probability for a molecular dipole to reorient is described by the Arrhenius formula as seen in Fig. 6. The deviation observed in the H relaxation process at low temperatures in Fig. 6 coincides with the conspicuous asymmetry of $\epsilon''(f)$ curves seen in Figs. 3(f) and 4(f); both the deviation and asymmetry are reasonably ascribed to the biaxial order growing stronger in the tilted smectic phases at lower temperatures with a consequent increase in barrier height to rotations due to an increase in the slope of the H-curve at lower temperatures in Fig. 5.

The emergence of the spontaneous polarization in the chiral tilted smectic phases and a possibility to induce the polarization in SmA near the phase transition temperature are the signatures of the correlated dipole motion in an entire smectic layer. In fact, the soft mode is usually observed in SmA and SmC^* but becomes weak rapidly with increasing tilt angle; the Goldstone mode is usually much stronger than the soft mode when the tilt angle is sufficiently large. In the MC881-MC452 mixture under investigation, a tilt angle as large as 20° or more suddenly appears just below SmA in the chiral tilted smectic phase, which is considered to be almost SmC^* with $q_T \simeq 1$; hence the Goldstone mode alone is observed in Figs. 3(a) and 3(b), although the soft mode emerges in SmA as indicated in Fig. 3(a). Since the spontaneous polarization appears parallel to the smectic layer in SmC^* and SmA, both soft and Goldstone modes are usually not observed in the homeotropic cell. On the other hand, the molecular dipole's reorientation processes around the molecular long and short axes, i.e., the H and L modes, can be observed in both planar and homeotropic cells; actually, however, the L mode could not be seen when the Goldstone mode is strong as in Figs. 3(a) and 3(b). Even in SmA, it is masked by the soft mode as in Fig. 3(a) but we can see it in the homeotropic cell as in Fig. 4(a); hence we can plot both modes separately in Fig. 5, although their resonant frequencies are rather close to each other.

In antiferroelectric SmC_A^*, the spontaneous polarization emerges but macroscopically it is canceled out. The in-phase and antiphase modes of fluctuations appear due to the unit cell structure consisting of two anticlinic smectic layers. The antiphase mode induces spontaneous polarization and hence couples with an applied electric field. In dielectric measurements the antiphase relaxation mode is observed in planar cells, at an in-between frequency of the molecular rotational modes, with moderate intensity stronger than the molecular rotational modes but much weaker than the Goldstone mode of SmC^* [10,11]. As seen in Figs. 3(c)–3(f), it is to be noted that the M mode appears stably over a wide temperature range from $\approx$80 °C down to room temperature or lower and hence corresponds to the subphase which Sandhya *et al.* found by observing the Bragg reflection spectra systematically [25–27]. In the previous consideration summarized in Sec. I, some ambiguity remains whether this subphase is $q_T = 1/3$ or $1/2$. Suppose it is $1/3$ and hence is ferrielectric; the M mode should be much stronger as there would exist spontaneous polarization macroscopically in contrast to the relatively weak mode being observed here. Therefore we can reasonably identify it as the antiferroelectric $q_T = 1/2$ subphase with the four-layer unit cell; we earnestly hope that this identification will be confirmed much more directly by carbon resonant x-ray scattering.

It may be wondered why the antiphase relaxation mode was detected even in the homeotropic cell as shown in Figs. 4(d) and 4(e). This is probably due to the spontaneous polarization emerging perpendicularly to the smectic layer. Notice that the spontaneous polarization is always parallel to the smectic layer in ordinary SmC^* and SmC_A^* [1,2]. In subphases such as $q_T = 1/3$ and $1/2$, however, Emelyanenko and Osipov [16] showed that the discrete flexoelectric polarization in the smectic layer i can be written as

$$\mathbf{P}_{\mathrm{f}}^{(i)} = -\tilde{c}_{\mathrm{f}}^{(1)} \cos\theta \, \Delta\mathbf{n}_{i\pm1} - \tilde{c}_{\mathrm{f}}^{(2)} \cos\theta \, \mathbf{n}_i (\Delta\mathbf{n}_{i\pm1} \mathbf{n}_i); \quad (2)$$

they appropriately assumed that the biaxiality is weak and that the tilt angle θ is the same for all smectic layers in subphases. The discrete flexoelectric polarization due to the first term with $\tilde{c}_{\mathrm{f}}^{(1)}$ coefficient is always parallel to the smectic layer i because it is proportional to the difference $\Delta\mathbf{n}_{i\pm1} \equiv \mathbf{n}_{i+1} - \mathbf{n}_{i-1}$. By contrast, the second term with $\tilde{c}_{\mathrm{f}}^{(2)}$ coefficient contains a contribution perpendicular to the smectic layer, although they ignored a small contribution of this term in their detailed subphase studies of Ref. [16]. Since the antiphase relaxation mode detected in the homeotropic cell may indicate the existence of perpendicular polarization due to the discrete flexoelectric effect, it would be interesting to perform the dielectric spectroscopic investigations of subphases in homeotropic cells systematically.

V. DISCUSSION

In this way the dielectric investigations performed support the previous conclusion that a single subphase emerges in a wide temperature range and furthermore indicate that this subphase is antiferroelectric, which is different from SmC_A^* and probably has the four-layer $q_T = 1/2$ structure (hereafter simply designated as the $q_T = 1/2$ subphase). In fact, we can see the typical antiphase relaxation mode in the wide temperature range from $\approx 80\,^\circ$C down to room temperature or lower as illustrated in Figs. 3 and 5. Within this wide temperature range we cannot see any discontinuous change in $\epsilon''(f)$; the peak shifts toward lower frequencies and the peak height increases continuously with falling temperature. On the other hand, conspicuous changes in $\epsilon''(f)$ are observed at the transitions among SmA, the SmC^*-like phase, and the $q_T = 1/2$ subphase; even the L mode of the molecular rotational motion around the short axis shows a discontinuous change, though very small, at these transition points. In particular, the dielectric amplitude $\Delta\epsilon$ as a function of temperature becomes characteristic after transition from the $q_T = 1/2$ subphase to the SmC^*-like phase, indicating that the SmC^*-like phase is more appropriately designated as the state with q_T quasicontinuously increasing with temperature (hereafter abbreviated as *the state with quasicontinuous* q_T). We explain the details in Sec. V A. At temperatures below zero and in low frequencies, the antiphase relaxation mode shows irregularities. It becomes stronger with falling temperature and shows a maximum at about $-4\,^\circ$C; furthermore a shoulder appears on the high-frequency side. We contemplate what is going on in this low temperature and frequency range in Sec. V B. So long as the biaxial subphases alone are considered, the original treatment by Emelyanenko and Osipov [16] is self-consistent and useful. However, the optically uniaxial subphases may also appear even when the tilt angle is large and constant as was pointed out by Sandhya *et al.* [37]. In the last Sec. V C we show the newly obtained g-$\tilde{T}$ phase diagrams look completely different from the previous ones and refer to the characteristic behavior of the helical pitch $p(T)$ as well as $q_T(T)$ in the subphase with continuously increasing q_T.

A. Characteristic behavior of $\Delta\epsilon(T)$ in the state with quasicontinuous q_T

Sandhya *et al.* [25–27] concluded, as summarized in Sec. I, that $q_T > 1/2$ continuously increases with rising temperature in the state which emerges just above the $q_T = 1/2$ subphase. Actually, they first obtained the macroscopic helical pitch as a function of temperature $p(T)$, which well reproduces the experimentally observed one above the $q_T = 1/2$ subphase, and then determined q_T. The two premises they used are the Boltzmann distribution for the ratio of $[A]/[F]$ and the empirical relation $p(q_T)$ with experimentally estimated helical pitches of SmC_A^* and SmC^*. Although it takes considerable time and work to determine $p(T)$ experimentally, it is much easier to check $p(T)$ in the state with quasicontinuous q_T as well as in the $q_T = 1/2$ subphase by measuring the optical rotatory power (ORP). Figure 7 shows the ORP as a function of temperature in the MC881 mixture containing 55.09 wt % MC452; the mixture from the same lot is used

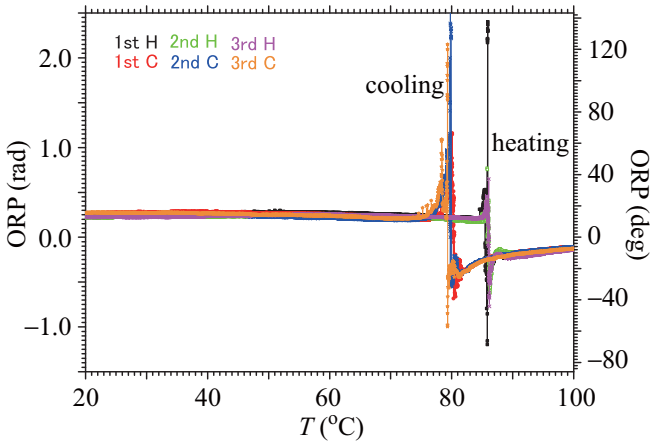

FIG. 7. The ORP as a function of temperature in a 30-μm-thick cell of MC881 mixture containing 55.09 wt % MC452 measured in the heating and cooling processes at a rate of 4.5 °C/h. The light source used is a He-Ne laser (633 nm).

in measurement (1) of Table I. Three results consecutively measured almost coincide with one another, although the ORP itself appears to fluctuate intrinsically. It is almost constant in the $q_T = 1/2$ subphase and starts to increase steeply at about 85 °C where the transition occurs from the $q_T = 1/2$ subphase to the state with quasicontinuous q_T. It becomes zero in-between $\pm\infty$ (maximum and minimum) where the helical pitch diverges and EFIB contours show a valley at $q_T \approx 0.6$ [25,38]; q_T increases with rising temperature as illustrated in Fig. [13] of Ref. [25].

Figure 8 is the dielectric amplitude as a function of temperature $\Delta\epsilon(T)$ obtained by using the data in measurement (1) of Table I. It looks like $q_T(T)$ in the state which emerges just above the $q_T = 1/2$ subphase as illustrated in Fig. 13 of Ref. [25]. We now consider why $\Delta\epsilon(T)$ resembles $q_T(T)$ in the state with quasicontinuous q_T. A system at nonzero temperature does not stay in its equilibrium mesoscopic state, but instead randomly samples all possible states. A 30-μm-thick cell has $[A] + [F] \approx 10^4$ as the layer spacing is about

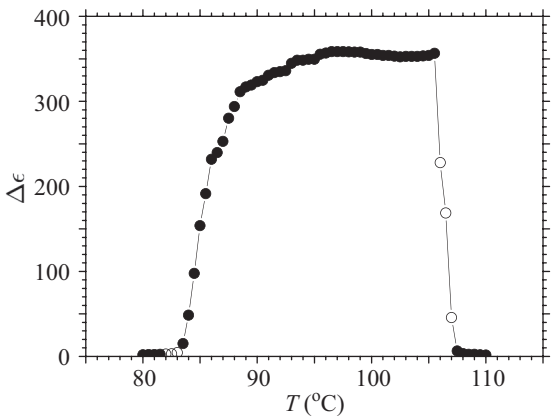

FIG. 8. The dielectric amplitude as a function of temperature, $\Delta\epsilon(T)$, in the temperature range of the state with quasicontinuous q_T and its vicinity. The two adjacent phases seem to coexist in the temperature ranges where $\Delta\epsilon$ is plotted by open circles.

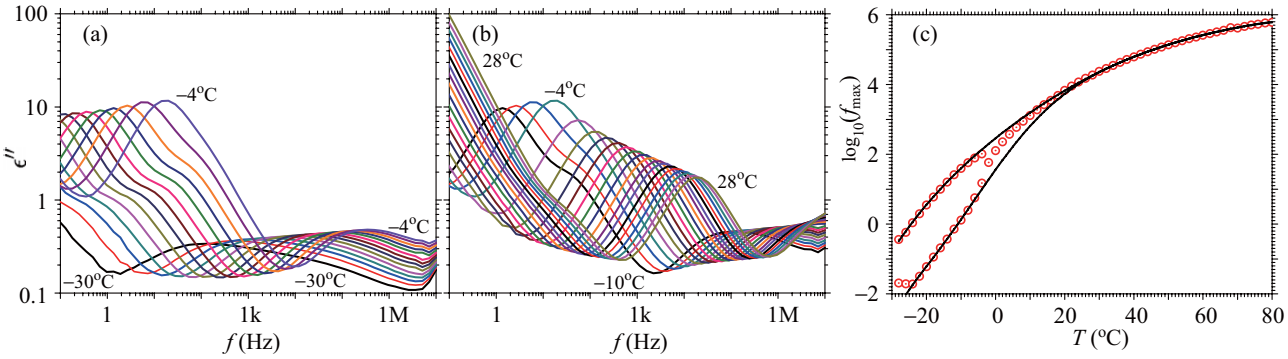

FIG. 9. The antiphase mode splitting at the low temperature and frequency range obtained in measurement (3) of Table I. To make it clear to see the temperature variation by avoiding the excessive overlapping of curves, $\epsilon''(f)$ in two temperature ranges are separately plotted for (a) -30 to $-4\,^{\circ}$C and (b) -10 to $28\,^{\circ}$C. (c) The logarithm of the antiphase mode relaxation frequency $\log_{10}(f_{\max})$ is also plotted as a function of temperature. Open circles were obtained by WinFIT on the assumption that the shoulders emerge at temperatures $T \leqslant -4\,^{\circ}$C but not for $T \geqslant -2\,^{\circ}$C. On the other hand, solid lines are drawn tentatively by considering that the antiphase mode peak gradually splits up over a wide temperature range. See text for further details.

3 nm. Each mesoscopic state with the same q_T value should appear with an equal *a priori* probability; some of them are ferrielectric and the others are antiferroelectric. Since an applied electric field selectively determines the director tilting sense, we should use $q_E = |[R] - [L]|/([R] + [L])$ instead of q_T; $[R]$ and $[L]$ refer to the numbers of smectic layers with directors tilted to the right and to the left, respectively. Within a large number of mesoscopic states in the macroscopic state with a particular value of q_T, the mesoscopic states with larger q_E's must contribute predominantly to the dielectric amplitude $\Delta\epsilon$. Since the largest q_E is equal to q_T of the macroscopic state, the temperature variation of the dielectric amplitude $\Delta\epsilon(T)$ looks similar to that of q_T in the state with quasicontinuous q_T.

B. The antiphase mode behavior in the low temperature and frequency range

Figures 9(a) and 9(b) are $\epsilon''(f)$ obtained in measurement (3) of Table I for $-30\,^{\circ}$C to $28\,^{\circ}$C at a step of $2\,^{\circ}$C. To make it clear to see the temperature variation by avoiding the excessive overlapping of curves, $\epsilon''(f)$ in two temperature ranges are separately plotted for (a) $-30\,^{\circ}$C to $-4\,^{\circ}$C and (b) $-10\,^{\circ}$C to $28\,^{\circ}$C. At temperatures below $0\,^{\circ}$C and low frequencies, the antiphase relaxation mode shows irregularities. It becomes stronger with falling temperature and attains a maximum at $-4\,^{\circ}$C. We now contemplate what is going on in this low temperature and frequency range. When we glance over Figs. 9(a) and 9(b), $\epsilon''(f)$ at a temperature lower than $-4\,^{\circ}$C has a shoulder, which becomes smaller with falling temperature. At $-6\,^{\circ}$C the peak and shoulder appear around 6 and 70 Hz, respectively. Even at $-4\,^{\circ}$C we can discern a shoulder, though not conspicuously, on the high-frequency side of the peak. On the other hand, we did not perceive any shoulder at $-2\,^{\circ}$C at first. Therefore we analyzed $\epsilon''(f)$ in Figs. 9(a) and 9(b) by WinFIT on the assumption that the shoulders emerge at temperatures $T \leqslant -4\,^{\circ}$C but not for $T \geqslant -2\,^{\circ}$C, and obtained open circles in Fig. 9(c). A phase transition appears to occur at a temperature between $-4\,^{\circ}$C and $-2\,^{\circ}$C where the peak is highest and the shoulder begins to appear. Actually, however, the phase transition seems to be caused by the above inappropriate fitting procedure; we need to analyze the original $\epsilon''(f)$ data given in Figs. 9(a) and 9(b) carefully.

When we look at the $\epsilon''(f)$ curve at $-2\,^{\circ}$C deliberately, it is clearly asymmetric and looks like having a shoulder or being composed of two subpeaks. Even the curves at higher temperatures than $-2\,^{\circ}$C have the similar tendency, although the asymmetry gradually diminishes with increasing temperature. It would be reasonable to consider that the antiphase mode peak gradually splits up over a wide temperature range. With this intention we tentatively draw two solid-line curves as in Fig. 9(c); *the shoulder on the high-frequency side* in the $T \leqslant -4\,^{\circ}$C range corresponds to the main peak at the higher temperature range, and *the shoulder on the low-frequency side* begins to emerge at around $20\,^{\circ}$C to $30\,^{\circ}$C and grows into the main peak in the $T \leqslant -4\,^{\circ}$C range. We suspect that the splitting is closely related with the two conceptual processes producing tilted smectic phases such as SmC^* and SmC_A^*: (1) the directors tilt relative to the fixed layers and (2) the layers tilt with respect to the fixed directors [39]. The supposition is based on the fact that the $q_T = 1/2$ subphase under investigation requires the frustration of SmC_A^* not only with SmC^* at higher temperatures but also with HeI^* or reentrant SmC^* at lower temperatures [27]; the hexatic character gradually develops in SmC_A^* with falling temperature. In such cases a tendency is developed that the smectic layer spacing becomes larger and the average tilt angle of molecular long axes with respect to the SmA layer normal decreases with falling temperature [40]. Actually the smectic layer spacing measured by x-ray scattering increases with decreasing temperature as shown in Fig. 10; the average tilt angle of the molecular long axes is considered to decrease although the tilt angle is not actually measured by IR spectroscopy as was done previously by Korlacki *et al.* [40].

In this way it can be considered that not only the director cooperative motion but also the cooperative undulational motion of the smectic layer produces net spontaneous polarization in their antiphase modes which is coupled with an electric field in the dielectric measurement. The director

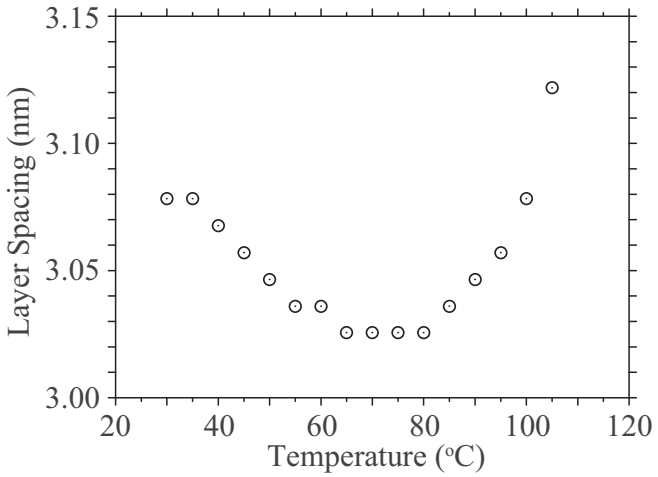

FIG. 10. Preliminary data of the temperature dependence of layer spacing obtained in the heating process at a rate of 10 °C/h.

cooperative motion in the antiphase mode has already been studied in detail experimentally [10–14,41] and theoretically [42–44] in connection with the pretransitional effect in the antiferroelectric phases; the averaged tilt plane direction may become parallel to the electric field and the directors in the unit cell may show some small asymmetric change to produce induced polarization in the initial averaged tilt direction, as intuitively illustrated in Fig. 1 of Ref. [45]. In fact, the director cooperative motion in the antiphase mode produces the net spontaneous polarization and hence operates in dielectric spectroscopy [10–14]. The effect of the cooperative undulational motion of the smectic layer in the antiphase mode on dielectric response, on the other hand, has not been studied up until now, as far as the authors are aware. Figure 11 illustrates how the smectic layers produce the net spontaneous polarization by moving cooperatively in the antiphase mode. Suppose the ordinary antiferroelectric four-layer $q_T = 1/2$ subphase [Fig. 11(a)] acquires the hexatic character, the smectic layers tend to tilt with respect to the fixed Sm*A* director and form

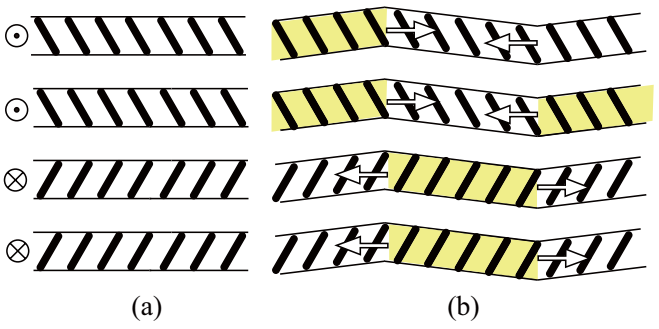

FIG. 11. Schematic illustrations of (a) the ordinary antiferroelectric four-layer $q_T = 1/2$ subphase and (b) the corresponding one with the hexatic character, where the smectic layers tend to tilt with respect to the fixed Sm*A* director and form zigzag structures. The cooperative undulational motion in the antiphase mode which expands the shaded area and reduces the other area produces net spontaneous polarization and plays an important role in dielectric spectroscopy. See text for details.

zigzag structures [Fig. 11(b)] [40]. The layer polarization increases locally in the favorable yellow shaded area where the director and the layer tilt in the same sense, whereas it decreases in the unfavorable area where they tilt oppositely; the net polarization in the unit cell naturally cancels out to assure antiferroelectricity in an equilibrium. The cooperative undulational motion in the antiphase mode produces net spontaneous polarization by enlarging the favorable area and diminishing the unfavorable one, and hence plays an important role in dielectric spectroscopy.

The director motion is mainly responsible for the dielectric response at high temperatures. As the temperature decreases, the layer undulational motion begins to participate in the dielectric response and becomes the main process at low temperatures, the resonance frequency $f_{\max}$ of which must be lower than that of the director motion. Therefore in Fig. 9(c) we can draw the two solid-line curves; in Figs. 9(a) and 9(b), in fact, the shoulder due to the layer undulational motion begins to emerge on the low-frequency side around 20 to 30 °C, grows bigger with falling temperature, and slowly becomes smaller below −4 °C. Notice that the shoulder on the high-frequency side at −4 °C is due to the director motion, and hence it should be connected to the main peaks at high temperatures. One thing we are uneasy about is a rather sudden change between 20 °C and 32 °C observed in measurement (4) as shown in Fig. 4(d); the change occurs around the temperature range where the two solid-line curves merge in Fig. 9(c). We need to repeat the measurement in homeotropic cells and check whether the sudden change is not an artifact. At the same time, for a better understanding of the antiferroelectric hexatic phase, it would be highly desirable to try to observe the layer undulational motion by dielectric measurements in much simpler SmC_A^* which was studied by x-ray scattering and IR spectroscopy in detail [40].

C. Degeneracy lifting due to LRILIs

Last but not least, it is important to remember that the LRILIs proposed by Emelyanenko and Osipov [16] hardly stabilize subphases with $q_T > 1/2$. The LRILIs are simple and effective in understanding the degeneracy lifting at the frustration point in the MC881-MC452 binary mixture system, where the tilt angle can be approximately considered constant as is already pointed out in Sec. IV. By considering subphase superlattice structures up to ten smectic layers, we obtained the g-$\tilde{T}$ phase diagrams as given in Fig. 12 of Ref. [27] which include the whole subphases experimentally observed so far [17,46]. Four dimensionless parameters are needed: g represents the molecular positional correlation in adjacent layers, $\tilde{T} = a\,(T - T^*)/(B\,T^*)$ the modified temperature, $c_{\rm f}/c_{\rm p}$ the ratio between flexoelectric and piezoelectric coefficients, and the final one $\chi c_{\rm p} c_{\rm f}/B$ represents the relative strength of the effective LRILIs. Thus we can explain the staircase character of the subphase emergence. As you see in the g-$\tilde{T}$ phase diagrams, many subphases with $q_T \leqslant 1/2$ have their reasonably wide emerging area, whereas subphases with $q_T > 1/2$ are squeezed into a narrow area. The staircase looks quite asymmetric with respect to $q_T = 1/2$. Moreover, the $q_T = 1/2$ subphase itself stably exists even at $g = 0$. In spite of the limited emergence of subphases with $q_T >$

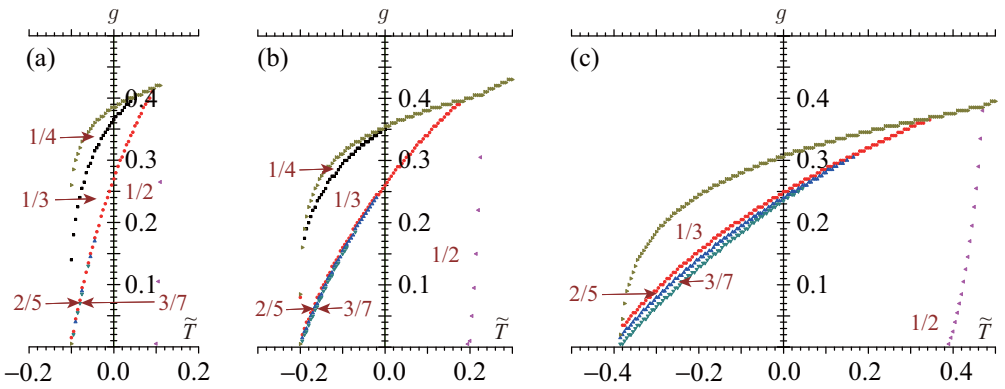

FIG. 12. The g-$\tilde{T}$ phase diagrams now look completely different from those previously obtained and shown in Fig. 12 of Ref. [27]. Parameters used are $c_f/c_p = 1.0$ and (a) $\chi c_p c_f/B = 0.05$, (b) 0.1, and (c) 0.2, respectively.

1/2, Emelyanenko and Ishikawa [47] insisted the importance of "Smooth transitions between biaxial intermediate smectic phases." On the other hand, the stable emergence of subphases with $q_T > 1/2$ would disturb the simple temperature dependence of the helical pitch $p(T)$ as well as $q_T(T)$ experimentally observed above the $q_T = 1/2$ subphase [25,27].

So long as the biaxial subphases alone are considered, their original treatment [16] is self-consistent and useful. It should be noticed, however, that optically uniaxial subphases may also appear even when the tilt angle is large and constant. In fact, Sandhya *et al.* [37] showed the following: When we treat the optically uniaxial subphase where the $\boldsymbol{c}$ director uniformly twists from layer to layer by $\Delta\varphi \equiv \varphi_{i+1} - \varphi_i$, the first term with $\chi c_p c_f/B$ representing LRILIs due to the discrete flexoelectric effect in Eq. (62) of Ref. [16] can be written as

$$\frac{\chi c_p c_f}{B}\frac{1}{1+2g\cos\Delta\varphi} \times\left(-\frac{1}{2}\frac{c_p}{c_f}+2\sin\Delta\varphi-2\frac{c_f}{c_p}\sin^2\Delta\varphi\right). \quad (3)$$

In the actual minimization process of the free energy, therefore, we need to know which of the biaxial and optically uniaxial subphases has the lowest free energy. In fact, we notice that purely anticlinic SmC_A^* and purely synclinic SmC^* are never stabilized; they automatically acquire the helical structures without considering an ordinary chiral interaction. Furthermore, as illustrated in Fig. 12, the g-$\tilde{T}$ phase diagrams now look completely different from those previously obtained and shown in Fig. 12 of Ref. [27]. Notice that subphases with $q_T < 1/4$ and $q_T > 1/2$ do not emerge. In this way, we recognize the legitimacy of the premises of Sandhya *et al.* [25] that the absolute zero temperature approximation does not hold anymore and that the thermal equilibrium between the synclinic and anticlinic orderings is given by the Boltzmann distribution.

VI. CONCLUSIONS

The subphase stabilized in an exceptionally wide temperature range has been studied by dielectric spectroscopy in two binary mixtures of antiferroelectric MC881 containing 55.09 and 55.70 wt % of ferroelectric MC452, respectively. The following six points are clarified:

(1) The subphase is surely antiferroelectric, since the antiphase relaxation mode is observed, which has probably the four-layer $q_T = 1/2$ structure.

(2) The antiphase relaxation mode splits gradually at low temperatures; one is due to the ordinary director cooperative motion, and the other should be caused by the cooperative undulational motion of the smectic layer that produces net spontaneous polarization.

(3) The antiferroelectric subphase stably exists down to $-30\,^\circ$C; no hexatic or reentrant SmC^* could be observed that was anticipated to exist previously [25,27].

(4) Just above the antiferroelectric subphase, there exists the state with quasicontinuous q_T; in fact, the dielectric amplitude gradually increases with temperature and indicates that each mesoscopic state with the same q_T value should appear with an equal *a priori* probability.

(5) The emergence of the $q_T = 1/2$ subphase and the state with quasicontinuous q_T results from the characteristic feature of the LRILIs proposed by Emelyanenko and Osipov and modified by Sandhya *et al.* [16,37].

(6) The antiphase relaxation mode detected in the homeotropic cell appears to indicate the existence of the polarization perpendicular to the smectic layer due to the discrete flexoelectric effect.

In this way, dielectric spectroscopy has additionally substantiated the counterintuitive stabilization of an antiferroelectric subphase (the $q_T = 1/2$ subphase) over an exceptionally wide temperature range and the emergence of the intriguing state with continuously increasing q_T with rising temperature (the state with quasicontinuous q_T), which are caused by a delicate balance of interlayer interactions and thermal fluctuations. We earnestly hope that the anticipated structure of four-layer $q_T = 1/2$ for the antiferroelectric subphase will be confirmed by carbon resonant x-ray scattering in the near future.

ACKNOWLEDGMENTS

MGC (Mitsubishi Gas Chemical Company, Inc.) is acknowledged for the gift of the precious liquid-crystal compounds, MC881 and MC452. Financial support from the

Ireland-Japan fund of Science Foundation Ireland (SFI) is acknowledged by J.K.V. The work of V.P.P. was partially supported by Brain Pool Program through the National Research Foundation of Korea (KR) ICT, 2019H1D3A2A02060963.

[1] R. B. Meyer, L. Liebert, L. Strzelecki, and P. Keller, J. Phys. Lett. (France) **36**, L69 (1975).
[2] A. D. L. Chandani, E. Gorecka, Y. Ouchi, H. Takezoe, and A. Fukuda, Jpn. J. Appl. Phys. **28**, L1265 (1989).
[3] J. Prost and R. Bruinsma, Ferroelectrics **148**, 25 (1993).
[4] R. Bruinsma and J. Prost, J. Phys. (France) **4**, 1209 (1994).
[5] A. Fukuda, Y. Takanishi, T. Isozaki, K. Ishikawa, and H. Takezoe, J. Mater. Chem. **4**, 997 (1994).
[6] M. Yamashita and S. Tanaka, J. Phys. Soc. Jpn. **68**, 1797 (1999).
[7] T. Matsumoto, A. Fukuda, M. Johno, Y. Motoyama, T. Yui, S.-S. Seomun, and M. Yamashita, J. Mater. Chem. **9**, 2051 (1999).
[8] M. Takeuchi, K. Chao, T. Ando, T. Matsumoto, A. Fukuda, and M. Yamashita, Ferroelectrics **246**, 1 (2000).
[9] J.-K. Song, A. Fukuda, and J. K. Vij, Phys. Rev. Lett. **101**, 097801 (2008).
[10] K. Hiraoka, H. Takezoe, and A. Fukuda, Ferroelectrics **147**, 13 (1993).
[11] M. Buivydas, G. Gauda, S. T. Lagerwall, and B. Stebler, Liq. Cryst. **18**, 879 (1995).
[12] K. Hiraoka, T. Tsumita, Y. Sugiyama, K. Monzen, Y. Uematsu, and Y. Suzuki, Jpn. J. Appl. Phys., Part 1 **36**, 6847 (1997).
[13] Y. P. Panarin, O. Kalinovskaya, and J. K. Vij, Liq. Cryst. **25**, 241 (1998).
[14] J.-K. Song, A. Fukuda, and J. K. Vij, Appl. Phys. Lett. **93**, 142903 (2008).
[15] M. A. Osipov and A. Fukuda, in *Abstracts of the Second Anglo-Japanese Seminar on Liquid Crystals, sponsored by British Liquid Crystal Society and Japanese Liquid Crystal Society* (York, UK, 2001) T–O6, p. 36.
[16] A. V. Emelyanenko and M. A. Osipov, Phys. Rev. E **68**, 051703 (2003).
[17] Z. Feng, A. D. L. Chandani Perera, A. Fukuda, J. K. Vij, K. Ishikawa, A. Iida, and Y. Takanishi, Phys. Rev. E **96**, 012701 (2017).
[18] P. Mach, R. Pindak, A.-M. Levelut, P. Barois, H. T. Nguyen, C. C. Huang, and L. Furenlid, Phys. Rev. Lett. **81**, 1015 (1998).
[19] P. Mach, R. Pindak, A.-M. Levelut, P. Barois, H. T. Nguyen, H. Baltes, M. Hird, K. Toyne, A. Seed, J. W. Goodby, C. C. Huang and L. Furenlid, Phys. Rev. E **60**, 6793 (1999).
[20] A.-M. Levelut and B. Pansu, Phys. Rev. E **60**, 6803 (1999).
[21] T. Akizuki, K. Miyachi, Y. Takanishi, K. Ishikawa, H. Takezoe, and A. Fukuda, Jpn. J. Appl. Phys., Part 1 **38**, 4832 (1999).
[22] P. M. Johnson, D. A. Olson, S. Pankratz, T. Nguyen, J. Goodby, M. Hird, and C. C. Huang, Phys. Rev. Lett. **84**, 4870 (2000).
[23] A. Cady, J. A. Pitney, R. Pindak, L. S. Matkin, S. J. Watson, H. F. Gleeson, P. Cluzeau, P. Barois, A.-M. Levelut, W. Caliebe, J. W. Goodby, M. Hird, and C. C. Huang, Phys. Rev. E **64**, 050702(R) (2001).
[24] I. Musevic and M. Skarabot, Phys. Rev. E **64**, 051706 (2001).
[25] K. L. Sandhya, A. D. L. Chandani, A. Fukuda, J. K. Vij, A. V. Emelyanenko, and K. Ishikawa, Phys. Rev. E **87**, 012502 (2013).
[26] K. L. Sandhya, A. D. L. Chandani-Perera, A. Fukuda, J. K. Vij, and K. Ishikawa, Europhys. Lett. **90**, 56005 (2010).
[27] A. Fukuda, Mol. Cryst. Liq. Cryst. **610**, 1 (2015).
[28] J. K. Song, A. Fukuda, and J. K. Vij, Phys. Rev. E **78**, 041702 (2008).
[29] J. Li, H. Takezoe, and A. Fukuda, Jpn. J. Appl. Phys. **30**, 532 (1991).
[30] P. Gisse, V. L. Lorman, J. Pavel, and H. T. Nguyen, Ferroelectrics **178**, 297 (1996).
[31] J. P. F. Lagerwall, F. Giesselmann, and M. Osipov, Liq. Cryst. **33**, 625 (2006).
[32] A. V. Emelyanenko, A. Fukuda, and J. K. Vij, Phys. Rev. E **74**, 011705 (2006).
[33] A. Fukuda, in *Proceedings of the Fifteenth International Display Research Conference*, Asia Display '95 Hamamatsu (The Institute of Television Engineering of Japan and The Society for Information Display, 1995), p. 61.
[34] Y. Yoshioka, M. Johno, T. Yui, and T. Matsumoto, European Patent Application No. EP1039329 (2000).
[35] T. Matsumoto (private communication, Washington, 2001).
[36] B. P. McGettrick, J. K. Vij, and C. B. McArdle, Int. J. Adhes. Adhes. **14**, 211 (1994).
[37] K. L. Sandhya, J. K. Vij, A. Fukuda, and A. V. Emelyanenko, Liq. Cryst. **36**, 1101 (2009).
[38] Z. Feng and K. Ishikawa, Jpn. J. Appl. Phys. **55**, 050301 (2016).
[39] G. Grinstein and R. A. Pelcovits, Phys. Rev. A **26**, 2196 (1982).
[40] R. Korlacki, A. Fukuda, and J. K. Vij, Europhys. Lett. **77**, 36004 (2007).
[41] M. Johno, K. Itoh, J. Lee, Y. Ouchi, H. Takezoe, A. Fukuda, and T. Kitazume, Jpn. J. Appl. Phys. **29**, L107 (1990).
[42] T. Qian and P. L. Taylor, Phys. Rev. E **60**, 2978 (1999).
[43] L. A. Parry-Jones and S. J. Elston, Phys. Rev. E **63**, 050701(R) (2001).
[44] L. A. Parry-Jones and S. J. Elston, Appl. Phys. Lett. **79**, 2097 (2001).
[45] A. D. L. Chandani, A. Fukuda, J. K. Vij, Y. Takanishi, and A. Iida, Phys. Rev. E **93**, 042707 (2016).
[46] A. D. L. Chandani Perera, A. Fukuda, J. K. Vij, and Y. Takanishi, Liq. Cryst. **44**, 1787 (2017).
[47] A. V. Emelyanenko and K. Ishikawa, Soft Matter **9**, 3497 (2013).